The Effects of Changing the Solar Constant on the Climate of a General Circulation Model

RICHARD T. WETHERALD AND SYUKURO MANABE

Geophysical Fluid Dynamics Laboratory/NOAA, Princeton University, Princeton, N.J. 08540

(Manuscript received 5 May 1975, in revised form 2 July 1975)

ABSTRACT

A study is conducted to evaluate the response of a simplified three-dimensional model climate to changes of the solar constant. The model explicitly computes the heat transport by large-scale atmospheric disturbances. It contains the following simplifications: a limited computational domain, an idealized topography, no heat transport by ocean currents, no seasonal variation, and fixed cloudiness.

It is found that the temperature of the model troposphere increases with increasing solar radiation. The greatest increase occurs in the surface layer of higher latitudes due to the effects of the snow-cover feedback mechanism as well as the suppression of vertical mixing by a stable lower troposphere. This result is found to be qualitatively similar to that obtained from previous studies with one-dimensional zonal mean models.

One of the most interesting features of this investigation is the extreme sensitivity of the intensity of the computed hydrologic cycle to small changes of the solar constant. Current estimates indicate a 27% increase of the former as compared with a 6% increase of the latter. This large intensification of the hydrologic cycle in the model atmosphere results from the increase in the rate of evaporation which is caused by the following changes: 1) reduction of the Bowen ratio due to the nonlinear increase of saturation vapor pressure with increasing temperature at the earth's surface, and 2) decrease in the net upward terrestrial surface radiation resulting from the increase in the moisture content in air and from the reduction of the lapse rate (both of which increase the downward terrestrial radiation and increase the energy available for evaporation).

It is shown that the latitude of maximum snowfall retreats poleward as the solar constant is increased. Furthermore, the total amounts of snowfall and snow accumulation decrease markedly with increasing insolation due to the poleward shift of the region of subfreezing surface temperature away from the zone of maximum baroclinic instability.

1. Introduction

One of the most important factors controlling the climate is solar radiation. Therefore, it is desirable to know how the climate responds to changes in the solar constant before investigating the mechanism of climate change.

A very crude estimate of the sensitivity of the equilibrium temperature of the atmosphere to the change in solar constant may be obtained from the equation

$$\delta T_e = \frac{1}{4}\left(\frac{1-\alpha}{4\sigma}S_0\right)^{\frac{1}{4}}\left(\frac{\delta S_0}{S_0}\right),$$

where α is the planetary albedo, S_0 the solar constant, σ the Stefan-Boltzmann constant, and δT_e the change of equilibrium temperature responding to the fractional change in solar constant $\delta S_0/S_0$. Assigning the value of 0.3 for the planetary albedo, one obtains a 0.6°C change in equilibrium temperature for a 1% change in the solar constant.

Manabe and Wetherald (1967) investigated a similar problem by use of a model of radiative, convective equilibrium of the atmosphere. They found that the dependence of the surface temperature upon the solar constant is twice as large as the values determined above when they take into consideration the change in water vapor content in air responding to the change in air temperature. In other words, the positive feedback between the greenhouse effect of water vapor and air temperature increases the sensitivity by a factor of approximately 2.

Budyko (1969) and Sellers (1969) constructed a simple, one-dimensional, zonal mean model of the atmosphere in which the influence of snow cover upon the albedo of earth's surface is taken into consideration. The effects of the poleward transport of heat due to atmospheric and oceanic circulation are incorporated in a highly parameterized form. They found that the positive feedback mechanism between the surface temperature and snow cover increases the sensitivity of their climate models. For example, a relatively small decrease in incoming solar radiation is sufficient for the development of an extensive ice sheet in their model. Budyko speculated that the frequent glaciations which occurred during the quaternary resulted from the change in solar radiation caused by the variation of turbidity in the atmosphere. In addition, he suggested that the secular change in the mean temperature of the earth's surface

during the last 100 years is also caused by the change in the turbidity of the atmosphere.

Most recently, Held and Suarez (1974) made a theoretical analysis of Budyko's model. They found that increasing the efficiency of poleward heat transport increases the sensitivity of this model to the change in the solar constant. In short, their results underscore the inportance of the accurate parameterization of the effect of heat transport in both the atmosphere and the ocean.

The present study represents a preliminary attempt to replace the parameterization of the effect of heat transport by explicit computation in a three-dimensional model of the atmosphere. The model which is used for this study, however, contains many simplifications or idealizations. For example, it has a limited computational domain ($\frac{1}{6}$ of the globe) and highly idealized distributions of ocean and continent. The heat transport by ocean currents is not taken into consideration. It is assumed that the distribution of cloudiness is not affected by the change in the solar constant. These simplifications have been made either because we have not found a proper formulation of the process involved or because they markedly reduce the computation time required. In view of these simplifications, it is not clear whether the present model yields more reliable results than the one-dimensional model constructed by Budyko. Therefore, the goal of this study cannot be the definitive evaluation of the sensitivity of climate to the change in the solar constant. Instead, we hope to find out whether a three-dimensional model with explicit dynamics of large-scale eddies behaves in a qualitatively similar manner to the one-dimensional models mentioned above. In addition, we hope to identify some of the important processes which play a major role in the change of climate.

One of the important mechanisms which is contained in the present model but not in most of the one-dimensional models is the hydrologic cycle. In this study, it is found that the intensity of the hydrologic cycle is very senstivie to the change in the solar constant. Therefore, special emphasis is placed upon the analysis of the response of hydrologic processes such as rates of precipitation and snow accumulation to the change in the solar constant.

This study follows the earlier work by Manabe and Wetherald (1975; hereafter referred to as MW75) on the sensitivity of the model climate to the change in the carbon dioxide content in air. Whenever appropriate, we intend to compare the results from the present study with those from MW75 in order to acquire a better appreciation of the behavior of the model.

2. Description of the model

The general circulation model used for this study is the same as that used in MW75. Detailed descriptions of the major components of the model may be found in Manabe (1969). Therefore, only a very brief description of the model is given here.

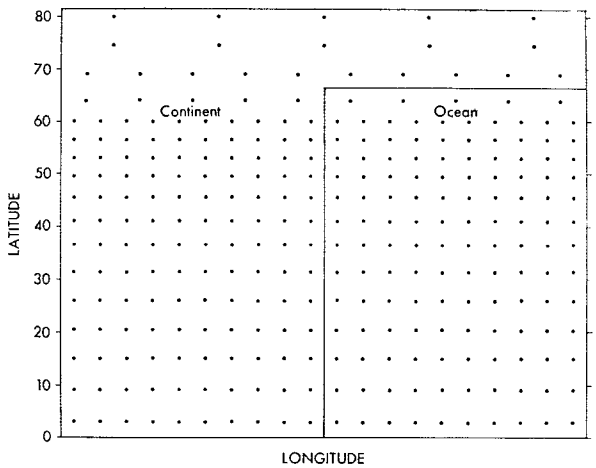

FIG. 1. Distribution of continent and ocean. Cyclic continuity is assumed from the eastern to western ends of the domain. Computational grid points in the space mesh are illustrated by dots.

The model solves the finite-difference form of the so-called "primitive equations of motion" on a Mercator projection. The contribution of subgrid-scale mixing is represented by nonlinear viscosity proposed by Smagorinsky (1963). The computational domain of the model which is used for this study is shown in Fig. 1. Free slip and insulated walls are placed at the equator and at 81.7°N, whereas cyclic continuity is assumed for the two meridional boundaries 120° of longitude apart. The domain is further divided into two areas, i.e., "continent" and "ocean." It should be stressed, however, that this model does not contain a separate oceanic model. The "ocean" is simply considered to be an area of wet swamp surface without any heat capacity. It resembles the actual ocean in the sense that it acts as a completely wet surface for evaporation but lacks the effects of heat transport by ocean currents.

Fig. 1 also illustrates the location of grid points chosen for the computation of finite differences. The average spacing of these grid points is ~500 km. To prevent the shrinkage of longitudinal grid size with increasing latitude, we reduced the number of grid points in the longitudinal direction at two selected latitudes. It was found that this abrupt reduction in computational resolution is responsible for the excitation of a computational mode and causes a sharp reduction of the magnitude of eddy kinetic energy and polward heat transport from the high to the low resolution side [see Appendix of Manabe (1969) for further details]. A model which avoids these difficulties is being developed at the present time (Holloway *et al.*, 1973). In the vertical direction, nine finite-difference levels are chosen so that the model can simulate the structure of both the stratosphere and the planetary boundary layer. The scheme for computing radiative heating and cooling is described by

Manabe and Strickler (1964) and Manabe and Wetherald (1967). It computes both solar and longwave radiation fluxes.[1] The distribution of cloudiness is specified from annual mean observations and is a function of latitude and height only. Three atmospheric gases are taken into account, i.e., water vapor, ozone and carbon dioxide. The distribution of water vapor used for the radiative computation is determined by the prognostic equations of the model. In this manner, the so-called "greenhouse-temperature feedback," which is mentioned in the Introduction, is taken into consideration. The distribution of ozone is specified as a function of latitude and height. The mixing ratio of carbon dioxide is taken to be constant everywhere. The surface temperature over the continent and the hypothetical ocean is determined from the boundary condition that no heat is stored at the earth's surface, i.e., net fluxes of solar and terrestrial radiation and the turbulent fluxes of sensible and latent heat locally sum to zero.

The prognostic system of water vapor involves the three-dimensional advection of water vapor, evaporation, vertical mixing, nonconvective condensation, and a so-called moist convective adjustment. Over continental surfaces, the depth of snow cover and the amount of soil moisture are based upon detailed balance computations of snow and soil moisture, respectively. In particular, the snow depth is increased by snowfall and depleted by sublimation and snowmelt. The latter quantity is computed from the requirement of the heat balance when conditions for the snowmelt are satisfied. Differentiation between rain or snow is determined by the temperature at a height of $\sim$350 m. If this temperature is equal to 0°C or below, precipitation is in the form of snow; otherwise, it occurs in the form of rain. Over the oceanic region, the area of sea ice is identified as the area where the surface temperature over the ocean is less than −2°C.

For the computation of the heat balance at the earth's surface, it is necessary to know the distribution of surface albedo. It is assumed that the albedo of the soil is a function of latitude and that its distribution with latitude is the same as that used by Manabe (1969). The albedos of snow and sea ice are assumed to be much larger than the albedo of bare soil. As pointed out in the Introduction, this difference in albedo induces the snow cover feedback.

Both snow cover and sea ice are classified into two categories, i.e., stable and temporary. Different values of albedo are assigned to eah category. According to the analysis by Budyko (1956), unstable snow cover and unstable sea ice are assigned an albedo of 0.45 and 0.35, respectively, whereas both stable snow cover and permanent sea ice are assigned a common albedo of 0.70. The discrimination between the stable and temporary snow cover (sea ice) is made according to the surface temperature of snow cover (sea ice). For the current study, this critical surface temperature was assigned a value of −25°C.

Originally, it was intended to assume this critical surface temperature to be −10°C. Because of a mistake in programming, the value of −25°C was actually used instead of −10°C. This error will have the effect of displacing poleward the boundary of the permanent ice cap with high albedo by approximately 10° latitude. However, one should note that the surface albedo of 70% yields a planetary albedo greater than the values determined from satellite observations over polar regions. Therefore, it is suggested in MW75 that the snow albedeo, which is determined by the erroneous code, can yield a more realistic planetary albedo than that from the correct code. For further discussion of the consequence of this code error, see Section 4d of the MW75.

3. Approach to equilibrium

As mentioned in the Introduction, the numerical experiments are performed for four different values of the solar constant: 2.04, 2.00, 1.96 and 1.92 ly min^{-1}. The standard value for the solar constant is taken to be 2.00 ly min^{-1} and the other three cases correspond to a 2% increase, 2% decrease, and 4% decrease of this standard value, respectively.

The methods of initialization and integration are identical with those employed for the carbon dioxide study described in MW75. Each case consists of two separate runs, starting from different initial conditions and integrated out for a period of approximately 800 model days. The equilibrium climates of the runs are obtained by averaging over the last 100-day periods and the final state of equilibrium for each case is obtained by averaging the two 100-day mean states. [See Section 3 and Appendix B of MW75 for further details of the time integrations and the evaluation of the degree of convergence obtained.]

It should be mentioned here that in climate studies of this nature, it is possible to obtain a quasi-equilibrium state which is considerably different from those discussed in this current investigation if either the external forcing (such as changes in the solar constant or carbon dioxide concentration) is larger than certain critical values or the initial conditions are too extreme. A preliminary evaluation of this problem is given in Appendix A where a brief analysis of such a case is presented.

One of the interesting results, which we noted in the course of the time integrations, is that the time required for convergence toward a state of equilibrium depends on the magnitude of the solar constant. Fig. 2 shows how the normalized value of mean temperature deviation approaches equilibrium states for two time integra-

[1] For this study, the scheme of computing radiative fluxes is calibrated such that it yields a balance between the area integral of net downward solar radiation and that of net upward terrestrial radiation, given the realistic distributions of temperature and humidity. For further details, see Appendix A of MW75.

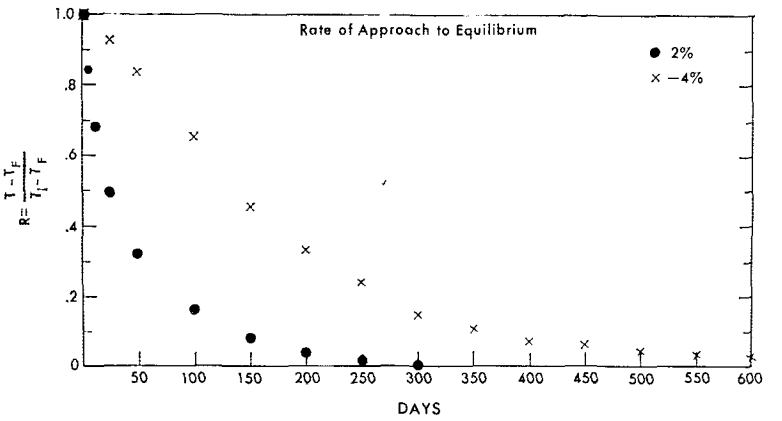

FIG. 2. Time plot of normalized values of mean temperature deviation defined by $(\bar{T}-\bar{T}_F)/(\bar{T}_I-\bar{T}_F)$, where $\bar{T}$ is mean (mass-weighted) temperature, and $\bar{T}_I$ and $\bar{T}_F$ are initial and final mean temperatures, respectively.

tions. This figure clearly reveals that the rate of convergence for the +2% case is much greater than the rate for the −4% case. In the study of the behavior of their zonal mean model, Held and Suarez (1974) discussed the stability of equilibrium states obtained from the model. They found that the thermal relaxation time involved in the approach toward an equilibrium state becomes longer as the value of the solar constant is reduced toward the critical value for inducing instability of the ice cap. According to their analysis, this difference in relaxation times is related to both the latitudinal position of the ice cap boundary and the amount of incident solar radiation at that particular latitude where the large change of surface albedo takes place. The lower the latitude of the ice cap boundary the greater the change in reflected radiation due to the change in albedo. Therefore, the net restoring force to small perturbations is weaker for an ice cap boundary located in lower latitudes as compared with an ice cap boundary located in higher latitudes. This mechanism is more complicated in our current study owing to the two types of snowcover boundaries involved (i.e., new snow and permanent ice) but it is nevertheless interesting that their result seems to be consistent with the behavior of the present model as described above. For a more complete discussion of this subject, refer to Section 3 of Held and Suarez (1974).

Finally, it should be pointed out that the thermal relaxation time which is implied by Fig. 2 is much less than the thermal relaxation time of a combined ocean-atmosphere model such as that developed by Manabe and Bryan (1969). Since the present model has an idealized swamp ocean without any heat capacity, its relaxation time is much shorter than that of a joint ocean-atmosphere model in which the ocean has a very large heat capacity. In order to obtain a quasi-equilibrium climate from a long-time integration of a joint model, it is necessary to develop a method of economical approach toward a quasi-steady state. [For further discussion of this subject, see Manabe and Bryan (1969).]

4. Change of the solar constant

This section deals with the comparison between the statistical equilibrium states corresponding to the four values of the solar constant considered in this study. For ease of identification, the four cases will be denoted as 0% (present solar constant), +2% (2% increase of the present solar constant), −2% (2% decrease of the present solar constant), and −4% (4% decrease of the present solar constant). Unless we specify otherwise, the results presented here are obtained by taking the average of two time mean states, computed from the last 100-day period of each integration.

a. Temperature

The first comparison concerns zonal mean temperature. For reference, the latitude-height distribution of zonal mean temperature for the 0% (standard) case is shown in Fig. 3a. Refer to MW75 for further discussion of this distribution.

Fig. 3b shows the difference in zonal mean temperature between the +2% and 0% cases. According to this figure, net warming takes place over most of the region responding to the increase of the solar constant. This warming is most pronounced in high latitudes because of the reduction of the area of snow cover with large surface albedo. In other words, the increase in the intensity of solar radiation raises the temperature of the earth's surface, reduces the area of snow cover, and thus causes the further increase of surface temperature. In addition to this positive feedback mechanism, there is another important reason for this large warming. According to Fig. 3b, the warming in high latitudes is essentially confined to a relatively shallow layer next to the earth's surface because of the suppression of

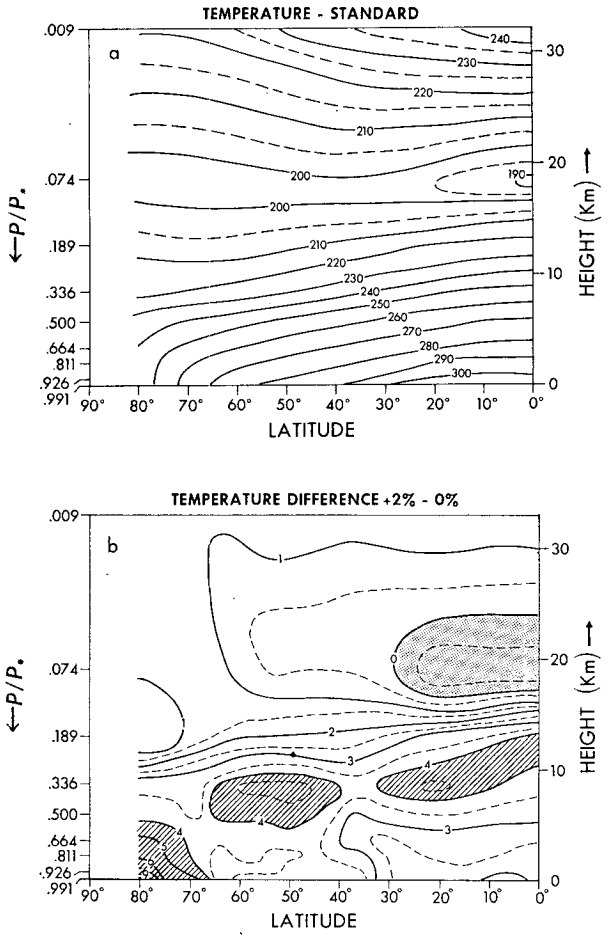

FIG. 3. Latitude-height distributions of the zonal mean temperature for the 0% (standard) case (a) and for the difference between the 2% and 0% cases (b). Stippling indicates a decrease in temperature. Units are in K.

vertical mixing in stable layers. Therefore, most of the thermal energy involved affects the temperature of this shallow surface layer rather than being spread throughout the entire depth of the troposphere. In the model tropics, the warming spreads throughout the entire troposphere, and its magnitude is relatively small as compared with the warming in the polar regions.

In lower latitudes of the model, the warming is greater in the upper troposphere (~336 mb) than near the surface. Qualitatively, the same feature was present in Fig. 4b of MW75 and results from the predominance of moist convection which adjusts temperatures in a vertical column toward the moist adiabatic lapse rate. Since the moist adiabatic lapse rate decreases with increasing temperature, the temperature of the upper troposphere increases more than that of the lower troposphere in lower latitudes where moist convection predominates.

It is interesting that the tropospheric warming responding to the 2% increase in the solar constant is comparable in magnitude to the tropospheric warming obtained for the doubling of CO_2 (see Fig. 4b of MW75). The main difference occurs in the stratosphere where the sign of the temperature change reverses between the two cases.

Fig. 4 illustrates the zonal-mean temperature at the lowest atmospheric level (991 mb) for the four separate cases (+2%, 0%, −2%, −4%), respectively. Two features are readily apparent:

1) There is a large increase of zonal mean surface temperature from −4% to +2% in higher latitudes, whereas there is a smaller change at equatorial latitudes.

2) The difference between successive cases decreases with increasing solar constant in higher latitudes.

From Fig. 4, it is obvious that the nonlinear dependence of surface temperature upon the solar constant is most apparent in higher latitudes where the area of snow cover decreases markedly with increasing solar constant. As mentioned in the Introduction, Budyko (1969) and Sellers (1969) investigated the climatic effects of the change of the solar constant by use of their one-dimensional models. They obtained nonlinear results which are qualitatively similar to those described above.

The observed zonal mean temperature distribution [taken from Oort and Rasmusson (1971) and shown as large dots in Fig. 4] indicates an interesting comparison with the present results. In all cases shown, the computed north-south temperature gradient is considerably greater than the observed one. One of the most important reasons for this discrepancy is the lack of poleward heat transport by ocean currents in the present model.

The sensitivity of the model described above is also reflected by the variation of global mean temperature. Table 1 shows the difference of global mean surface temperature as a function of solar constant variation for both the general circulation model and the associated radiative-convective equilibrium model constructed by Manabe and Wetherald (1967). The scheme for computing radiative transfer in the general circulation

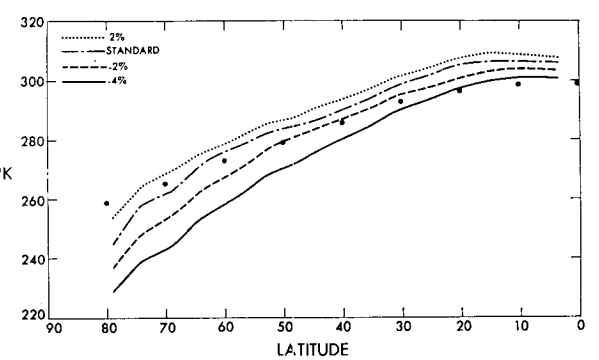

FIG. 4. Zonal-mean temperature at the lowest prognostic level (i.e., approximately 991 mb level) for all four cases. Dots indicate the observed distribution of zonal mean surface air temperature in the Northern Hemisphere (Oort and Rasmusson, 1971).

model is identical to that adopted by the radiative convective model of Manabe and Wetherald. Also shown for the sake of comparison are the corresponding values obtained by using a version of the Rodgers-Walshaw radiation model (1966) which is modified by Stone and Manabe (1968). Two facts are quite evident from this table: (i) the magnitude of the surface temperature differences are significantly greater for the general circulation model than for the radiative, convective model; and (ii) the functional relationship between mean surface temperature and solar constant is not linear for the general circulation model, whereas it is more linear for the radiative convective model.

In subsection 4d, it is shown that the area of snow cover in the general circulation model decreases nonlinearly with increasing solar constant. This is mainly responsible for the nonlinear response of surface temperature mentioned above. The closer correspondence between the results from the two models for the higher value of the solar constant is due to the reduction in the relative importance of the feedback mechanism between snow cover and surface temperature.

Fig. 5 illustrates how the nonlinear dependence of the area-mean temperature upon the solar constant varies with altitude. As expected, the greatest nonlinear variation is observed most clearly near or at the surface. This variation becomes more linear as the height is increased. This is because the lowest layers are directly influenced by the growth or decay of the snow-cover.

It should be noted here that both Budyko and Sellers have found a similar nonlinear response of surface temperature with their one-dimensional models. Furthermore, they found that, when the solar constant is reduced by more than a critical percentage, the ice cap of their model becomes unstable and extends all the way to the equator. This critical percentage is 1.5 for Budyko's model and 2–5 for Sellers' model. Recently, Held and Suarez (1974) have shown that this value depends very much upon the choice of various parameters contained in their model, i.e., albedo of snow cover or eddy diffusivity of heat. The results from the present

TABLE 1. Changes of the equilibrium temperature of the earth's surface resulting from the variation of the solar constant. R-W model: radiative-convective equilibrium model, which incorporates the modified version of the radiation scheme developed by Rodgers and Walshaw (1966); M-W model: radiative-convective equilibrium model of Manabe and Wetherald (1967); G-C model: the general circulation model described in this paper. The figures for the G-C model represent average values over the entire domain. Units are in K.

Change of solar constant (%)	R-W model	M-W model	G-C model
0 → +2	+2.25	+2.57	+3.04
0 → −2	−2.31	−2.55	−4.37
−2 → −4	−2.34	−2.54	−5.71

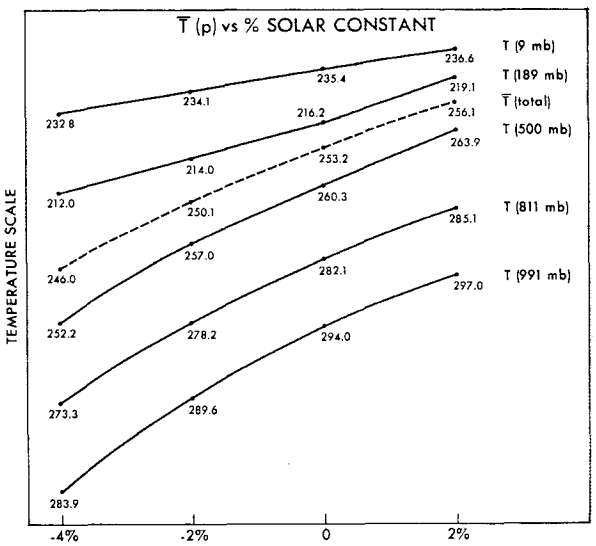

FIG. 5. Area-mean temperatures for various levels of the model as well as mass-weighted mean temperature for the total model atmosphere for each of the four cases. Vertical scale has been adjusted for each case separately and superimposed upon the others. Units are in K.

general circulation model suggest that the solar constant has to be reduced by more than 4% below the standard value to induce polar ice cap instability. As stated in the Introduction, it is not, however, reasonable to conclude that the present results are more reliable than the results from the one-dimensional studies mentioned above simply because our model treats the effect of heat transport explicitly rather than by parameterization. It should be noted here that our model not only suffers from insufficient computational resolution but also from the simplifying assumptions of fixed cloudiness, neglect of seasonal variation, and no oceanic heat transport. (Based upon the results from their simple model, Held and Suarez, for example, concluded that the incorporation of the effect of oceanic heat transport should significantly increase the sensitivity of the model climate to the variation of the solar constant.) Nevertheless, it seems to be significant that both the one-dimensional and three-dimensional models yield qualitatively similar results in many respects.

b. Relative humidity

The latitude-height distribution of relative humidity which emerged from the time integration of the model with the standard value of the solar constant is shown in Fig. 6a. This relative humidity distribution is identical with that presented as Fig. 6a in MW75 and is repeated here mainly for reference.

Fig. 6b shows the difference in zonal mean relative humidity between the +2% and −4% cases. According to this figure, the pattern is rather irregular. Therefore, the details of this distribution may not be significant.

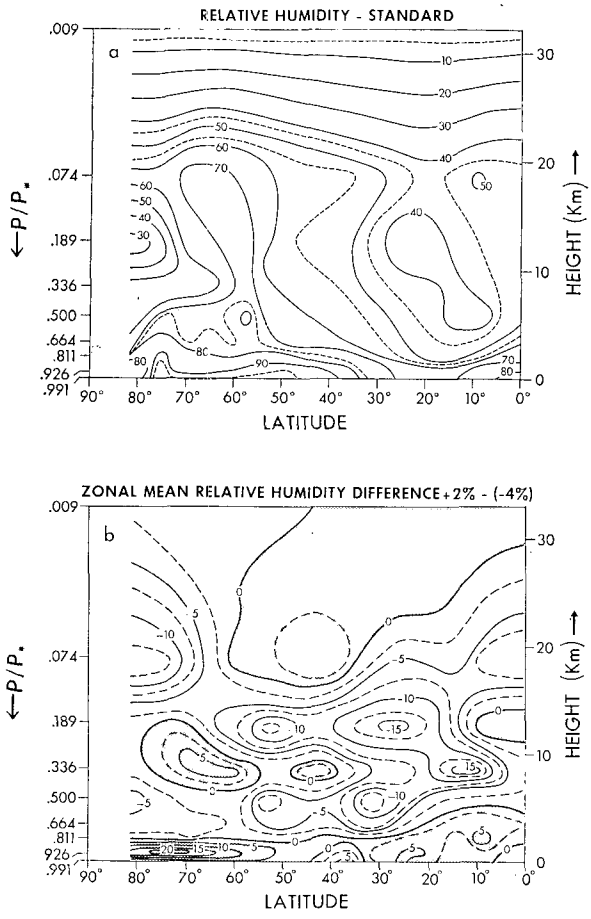

FIG. 6. Latitude-height distribution of zonal mean relative humidity for the 0% case (a) and for the difference between the +2% and −4% cases (b). Stippling indicates an increase in relative humidity. Units are in percent.

However, it is possible that the large-scale features of this difference are meaningful, because they are qualitatively similar to changes in relative humidity resulting from the doubling of carbon dioxide (see Section 4b, Fig. 6b, in MW75).

In general, relative humidity increases near the earth's surface and decreases in the middle and upper troposphere, responding to the increase in the solar constant. According to our speculation, the increase near the earth's surface results from the enhancement of evaporation from below, which is discussed in subsection 4c. On the other hand, the increase in the magnitude of downward as well as upward motion accompanied by the overall increase in the rate of precipitation may be responsible for the lowering of area mean relative humidity in the middle troposphere. (Note that, because of the process of precipitation, the drying in the region of subsidence tends to be larger than the moistening in the region of upward motion.)

Based upon his statistical analysis of cloudiness and upper atmosphere data, Smagorinsky (1960) shows that the relative humidities at different levels of the troposphere are related to the amounts of high, middle and low cloud. His results, together with those from Manabe and Wetherald (1967), suggest that the changes of relative humidity described above should have increased low cloudiness and decreased middle and high cloudiness if cloudiness is included as a prognostic variable of the model. As pointed out by Manabe and Wetherald (1967), cloud cover exerts two opposing effects upon the thermal structure of the model atmosphere in radiative, convective equilibrium. It reflects solar radiation and reduces the heat absorbed by the earth-atmosphere system. At the same time, cloud cover lowers the temperature of the effective source of upward emission into space and reduces the loss of heat due to terrestrial radiation. In general, the former (cooling effect) significantly exceeds the latter (heating effect) with the exception of high cloud which may raise or lower the temperature depending upon the details of its optical properties. Since we have not attempted the prediction of stratiform cloud in the present model, it is not obvious whether the change in cloudiness described above contributes to net heating or cooling. In view of the fact that low cloudiness has a particularly strong cooling effect, we suggest, however, that the changes in stratiform clouds described above may tend to counteract the original warming caused by the increase in the solar constant. On the other hand, it is probable that the increase in the rate of evaporation, which occurs as a responce to the increase of the solar constant (to be discussed in the following subsection), enhances the activities of moist convection, increases the overall height of cumuliform cloud, and thus raises the temperature of the model atmosphere. Construction of a scheme of accurate prediction of cloud cover is indispensable for evaluating the magnitudes of these opposing effects.

c. Hydrologic cycle and heat balance

One of the most notable aspects of this investigation is the apparent large sensitivity of the computed hydrologic cycle to relatively small changes of the solar constant. Description and discussion of this feature follows.

Fig. 7 shows the latitudinal distributions of zonal mean rates of precipitation and evaporation for the +2% and −4% cases. For both quantities, the rates for the +2% case are significantly greater than the corresponding rates for the −4% case over most of the region. Averaged over the entire computational domain, the time mean rates of precipitation are practically equal to those of evaporation. The values are 0.213 cm day^{-1} for the −4% case and 0.284 cm day^{-1} for the 2% case. This suggests that, within the limits of this study, the higher the value of the solar constant, the larger the amounts of precipitation and evaporation. The larger amount of insolation reaching the ground increases the heat energy available for the evaporation

from the earth's surface, and thus intensifies the hydrologic cycle in the model atmosphere. Qualitatively, the same results were obtained for the carbon dioxide study presented in MW75.

The change in precipitation rate resulting from the change in the solar constant is not uniform at all latitudes. According to Fig. 7, the magnitude of the change is particularly small in the subtropics and relatively large in middle latitudes of the model. The magnitude of the change in the evaporation rate varies less with respect to latitude than the change in precipitation rate with the exception of very high latitudes. It should be noted that the fractional change in evaporation rate is large in very high latitudes where the magnitude of evaporation rate itself is very small. This is due to the large reduction in saturation vapor pressure at the earth's surface resulting from the large cooling of surface temperatures. The reason for this will become evident when we discuss the change in the Bowen ratio in the latter part of this section. In addition to the distributions of the rates of precipitation and evaporation, the rate of snowfall is also shown in Fig. 7. This subject is not discussed here because it is covered extensively in subsection 4d.

Table 2 shows how the area-mean rate of precipitation depends on the magnitude of the solar constant.

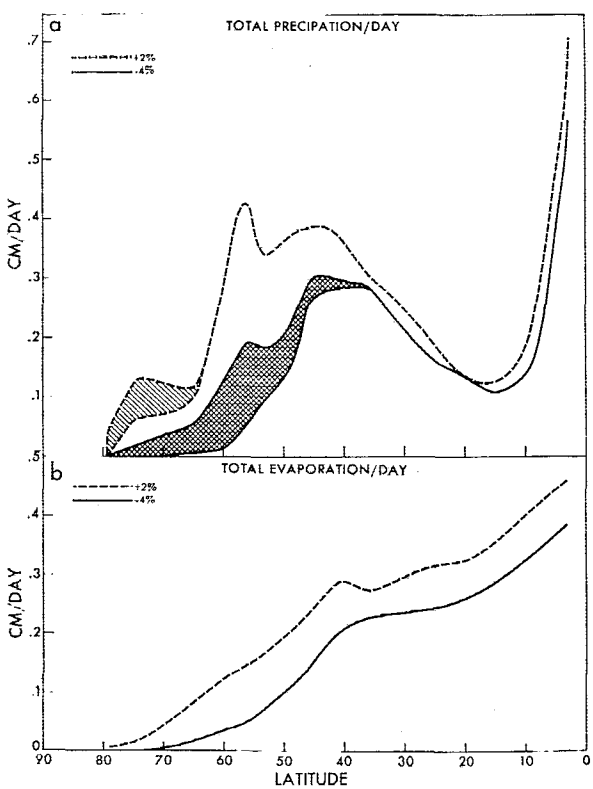

FIG. 7. Zonal mean rates of total precipitation (a) and evaporation (b) for the +2% and −4% cases. Shaded areas in (a) denote the rates of snowfall. Units are in cm day $^{-1}$.

TABLE 2. Area-mean rate of precipitation for the four different values of the solar constant considered in this study. Relative magnitude is defined as the ratio of the given rates to the rates corresponding to the 0% case.

Experiment	Solar constant (ly min^{-1})	Relative magnitude	Rate of precipitation (cm day^{-1})	Relative magnitude
+2%	2.04	(1.02)	0.284	(1.10)
0%	2.00	(1.00)	0.257	(1.00)
−2%	1.96	(0.98)	0.241	(0.94)
−4%	1.92	(0.96)	0.213	(0.83)

In this table, the rate of precipitation is listed not only in units of centimeters per day but also in a relative unit in which the precipitation rate for the 0% case is identified as 1.00. Since the evaporation rate is identical with the precipitation rate, it is not shown here. The precipitation rate represented in this relative unit may be regarded as an indication of the overall intensity of the hydrologic cycle in the model atmosphere. This table reveals the remarkable fact that the mean precipitation rate increases by as much as 27% in response to the 6% increase of the solar constant. In other words, the intensity of the hydrologic cycle in the model atmosphere changed 4.5 times as much as one would expect from the fractional change in the solar constant.

In order to clearly understand the mechanisms for the remarkable intensification of the hydrologic cycle mentioned above, it is essential to recall the following condition of heat balance which is satisfied at the surface of the model: the net downward radiation (net downward solar radiation minus net upward terrestrial radiation) at the surface is equal to the sum of sensible and latent heat fluxes. According to the results of our analysis, net upward terrestrial radiation decreases with increasing solar constant and contributes to the enhancement of evaporation by increasing the energy available for both evaporation and sensible heat fluxes as a whole. Futhermore, the increase of saturation vapor pressure at the earth's surface due to the warming of surface temperature increases the proportion of latent heat to sensible heat flux and intensifies the hydrologic cycle. The elaborations of these causes follow.

The first of the reasons concerns the variation of radiative fluxes at the surface of the model earth. According to Table 3, which shows the various components of heat balance in the model atmosphere, the following changes take place in response to a 6% increase in insolation: the net downward solar radiation at the surface *increases* by about 7% and the net upward terrestrial radiation *decreases* by about 8%. In other words, the percentage increase of the net insolation at the surface is slightly greater than the percentage increase in the solar constant. However, it is surprising that the net upward terrestrial radiation decreases significantly despite the increase in surface temperature.

TABLE 3. Heat balance components of the four model atmospheres considered in this study: SRT, incoming solar radiation at the top of the atmosphere; NSRT, net downward solar radiation at the top of the atmosphere; NLRT, net upward terrestrial radiation at the top of the atmosphere; NSRB, net downward solar radiation at the earth's surface; NLRB, net upward terrestrial radiation at the earth's surface; SH, upward flux of sensible heat; LH, upward flux of latent heat; C, condensation. Values given represent area means over the entire computational domain. Units are in ly min^{-1}. Numbers in parentheses indicate the relative magnitude as compared with the 0% (standard) case.

	Experiment			
	+2%	0%	−2%	−4%
SRT	0.510 (1.02)	0.500 (1.00)	0.490 (0.98)	0.480 (0.96)
NSRT	0.343 (1.03)	0.334 (1.00)	0.324 (0.97)	0.310 (0.93)
NLRT	0.343 (1.03)	0.334 (1.00)	0.324 (0.97)	0.310 (0.93)
NSRB	0.242 (1.02)	0.238 (1.00)	0.233 (0.98)	0.226 (0.95)
NLRB	0.087 (0.96)	0.091 (1.00)	0.093 (1.02)	0.095 (1.04)
SH	0.037 (0.95)	0.039 (1.00)	0.039 (1.00)	0.042 (1.08)
LH	0.118 (1.09)	0.108 (1.00)	0.101 (0.94)	0.090 (0.83)
C	0.118 (1.09)	0.108 (1.00)	0.101 (0.94)	0.090 (0.83)

This decrease in the net upward radiation makes more energy available for evaporation and is partly responsible for the intensification of the hydrologic cycle.

Since the water vapor content in the atmosphere generally increases with increasing air temperature, the downward longwave radiation also increases. This is one of the important reasons why net upward terrestrial radiation decreases with increasing solar constant as mentioned above. Another important factor which affects the downward radiation is the static stability of the atmosphere. Given the surface temperature, the smaller the lapse rate, the larger the downward radiation. Since the lapse rate in low latitudes of the model is essentially controlled by moist convection (see subsection 4a), it decreases with increasing temperature (note that the moist adiabatic lapse rate decreases with increasing air temperature). Therefore, the net downward radiation increases with increasing surface temperature. In short, both the increase of absolute humidity and decrease of the lapse rate contribute to the increase of downward radiation and accordingly to the reduction of net upward radiation at the earth's surface. In Appendix B the dependence of terrestrial radiation upon

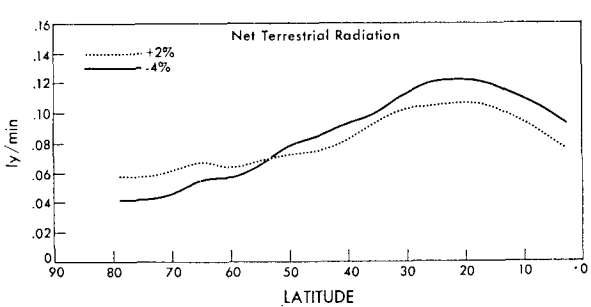

FIG. 8. Zonal mean net terrestrial radiation at the model surface for the +2% and −4% cases. Units are in ly min^{-1}.

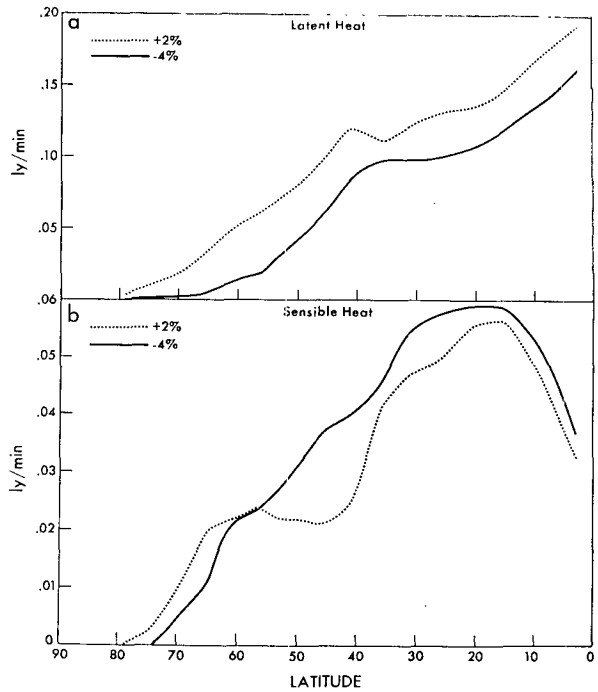

FIG. 9. Zonal mean latent heat flux (a) and sensible heat flux (b) at the model surface. Results are shown for both the +2% and −4% cases. Units are in ly min^{-1}.

the solar constant is discussed in further detail based upon the results from a radiative, convective equilibrium model of the atmosphere. Fig. 8 shows the latitudinal distributions of net upward terrestrial radiation at the surface for both the +2% and −4% cases. This figure indicates that the net terrestrial radiation for the +2% case is less than the corresponding flux for the −4% case except for a narrow polar region. In high latitudes where the surface temperature is low, the increase of the downward terrestrial radiation resulting from the increase in water vapor content of air is relatively small and is overcome by the increase in upward radiation due to the increase in surface temperature. Averaged over the entire area, the net upward terrestrial radiation decreases with increasing solar constant, as Table 3 indicates, despite this opposite contribution from the polar region.

The second reason for the large sensitivity of the hydrologic cycle concerns the change in the ratio of sensible heat to latent heat flux, i.e., the so-called Bowen ratio[2] at the ground surface of the model. According to Table 3, the following changes take place responding to the 6% increase in the solar constant: the sensible heat flux decreases by about 13% and the latent heat flux increases by about 26%. The linear increase in surface

[2] Bowen ratio $B=(C_p/L)(T_*-T_a)/(r_*-r_a)$, where the asterisk and a subscripts indicate the earth's surface and lowest prognostic level, respectively; C is the specific heat of air; L the latent heat of evaporation, T the temperature, and r the mixing ratio of water vapor.

temperature resulting from the increase in solar radiation raises the saturation vapor pressure nonlinearly at the earth's surface, thus enhancing the evaporation and making less energy available for sensible heat flux. (Note that the dependence of saturation vapor pressure upon temperature increases with increasing temperature.) This is why the sensible heat flux decreases despite the increase in radiative energy absorbed at the surface. In short, for a warmer surface temperature, the Bowen ratio is smaller and evaporation becomes a more effective means of removing heat from the surface than sensible heat flux. This is also evident in Fig. 9, which shows the latitudinal distribution of both latent and sensible heat fluxes. According to this figure, the latent heat flux increases at all latitudes in response to the increase in the solar constant. The opposite is true for sensible heat for all but high latitudes, where the surface temperature is low and the change in saturation vapor pressure to the variation of surface temperature is relatively small.

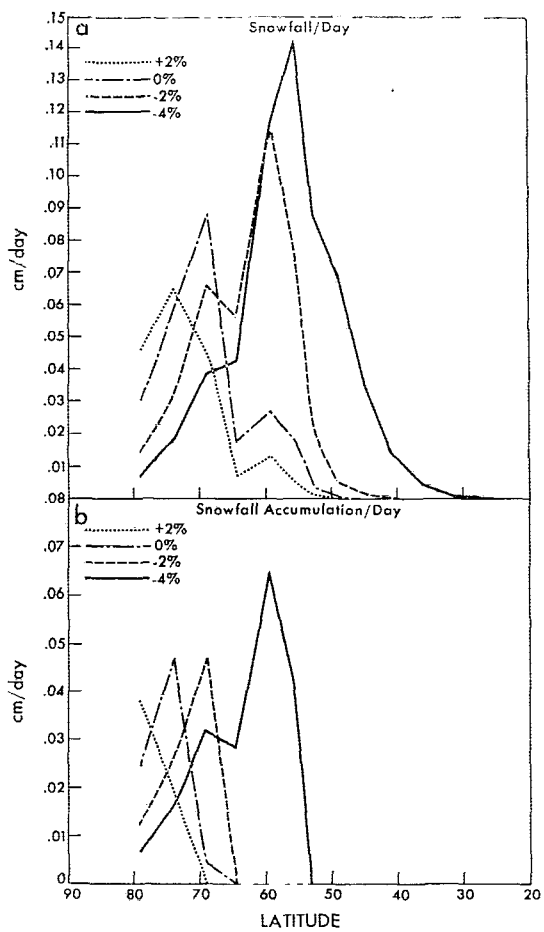

FIG. 10. Zonal mean rates of snowfall (a) and zonal mean rates of snow accumulation (b), each for all four cases. Units are in cm day^{-1}.

TABLE 4. Area-mean rate of snowfall for the four different values of the solar constant considered in this study. Relative magnitude is defined as the ratio of the given rates to the rates corresponding to the 0% case.

Experiment	Solar constant (ly min^{-1})	Relative magnitude	Rate of snowfall (cm day^{-1})	Relative magnitude
+2%	2.04	(1.02)	0.0047	(0.66)
0%	2.00	(1.00)	0.0071	(1.00)
−2%	1.96	(0.98)	0.0123	(1.73)
−4%	1.92	(0.96)	0.0209	(2.94)

d. Snowfall

The latitudinal distributions of the rates of snowfall are compared with those of rainfall for the +2% and −4% cases in Fig. 7. According to this figure, the area of snow cover decreases markedly with increase of the solar constant. Furthermore, the relative magnitude of the rate of snowfall as compared with the rate of total precipitation also decreases considerably. This decrease implies the net decrease of the total amount of snowfall despite the overall increase in the amount of precipitation discussed in the preceding section. This result seems to disagree with some of the speculations described in earlier publications. For example, Simpson (1934) speculated that the amount of snowfall increases with increasing solar radiation.

This matter may be examined further in Fig. 10a which shows how the distribution of snowfall is affected by the change in the solar constant. The following features are evident in this figure:

1) The latitude of maximum snowfall retracts poleward resulting from the increase in the solar constant.
2) The maximum rate of snowfall decreases with increasing insolation.

The first feature is a direct consequence of the poleward retreat of the zone of subfreezing surface temperature due to the increase of solar radiation. Such a retreat shifts the latitude of maximum snowfall away from the highly baroclinic zone in the middle latitudes where the rate of precipitation is at a local maximum due to the intense vertical velocity induced by cyclone waves. This is the main reason why the maximum rate of snowfall decreases markedly (second feature listed above) as the solar constant increases. Although the baroclinic belt shifts poleward in response to the increase in solar radiation, the magnitude of the shift is small and is much less than the magnitude of the retreat of the subfreezing zone (see Fig. 13). Therefore, the snowfall belt partly overlaps the belt of intense baroclinicity in the −4% case whereas the former is located at a much higher latitude than the latter in the +2% case.

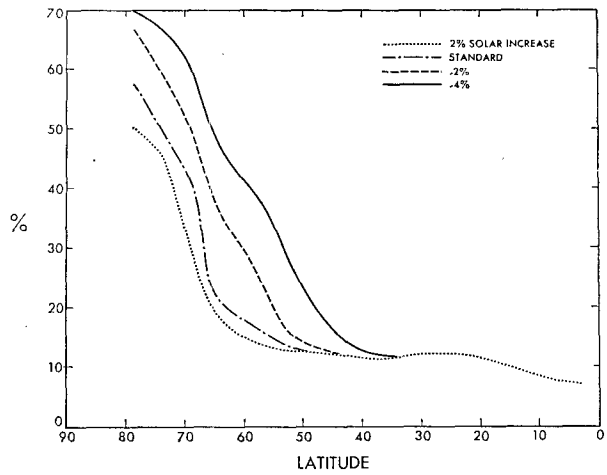

FIG. 11. Zonal mean surface albedo in units of percent for all four cases.

The dependence of the amount of snowfall on the solar constant is clearly demonstrated in Table 4 in which area-mean values of snowfall rate for the four cases are given. According to this table, the amount of snowfall decreases by a factor of as much as 2.3 in response to the 6% increase in the solar constant. The causes for this remarkable reduction have already been discussed in the preceding paragraph. One should also note that the poleward retreat of the region of snowfall results in a sharp reduction in the area of snowfall due to the shrinkage of the length of the latitude circle with increasing latitude. This factor can also be responsible for the sharp reduction of the amount of snowfall.

According to Fig. 10b, the latitudinal distribution of snow accumulation changes in a manner similar to that of snowfall in response to the change in the solar constant. This result implies that the snowfall essentially controls the qualitative features of the distribution of snow accumulation despite the large contribution of snowmelt to the budget of snow. It is interesting to speculate that, during ice ages, the thick ice sheet developed over the North American Continent by a similar mechanism, i.e., the penetration of the subfreezing zone into the baroclinic belt of middle latitudes.

In Section 4a, we stated that the warming caused by the increase of the solar constant is particularly pronounced in the polar region of the model because of the reduction of the snow-covered area with its large surface albedo. Fig. 11 shows the latitudinal distributions of surface albedo for each value of the solar constant considered in this study. This figure clearly shows that the area of large surface albedo in high latitudes decreases with increasing solar constant owing to the shrinkage of the area of snow cover.

e. Eddy kinetic energy

The latitude-height distribution of eddy kinetic energy for the standard case is shown in Fig. 12a. (Here, eddy kinetic energy is defined as the kinetic energy of the wind component representing the deviation from the zonal mean wind.) This figure is identical with Fig. 11a in MW75 which contains further discussion of this distribution.

Fig. 12b illustrates the difference of eddy kinetic energy between the +2% and the −4% cases. According to this figure, eddy kinetic energy decreases in the tropospheric layer below the 300 mb level in response to the increase of the solar constant. It is speculated that the eddy kinetic energy reduction results from the reduction of baroclinic instability caused by the change in the thermal structure of the model atmosphere. Examination of Fig. 3 reveals that the meridional temperature gradient decreases in the lower troposphere responding to the increase in the solar constant. Furthermore, the static stability increases in the lower troposphere of the middle and low latitudes. Both of these changes should suppress baroclinic instability. On the other hand, the static stability in the model atmosphere is less above the 300 mb level. This may be one

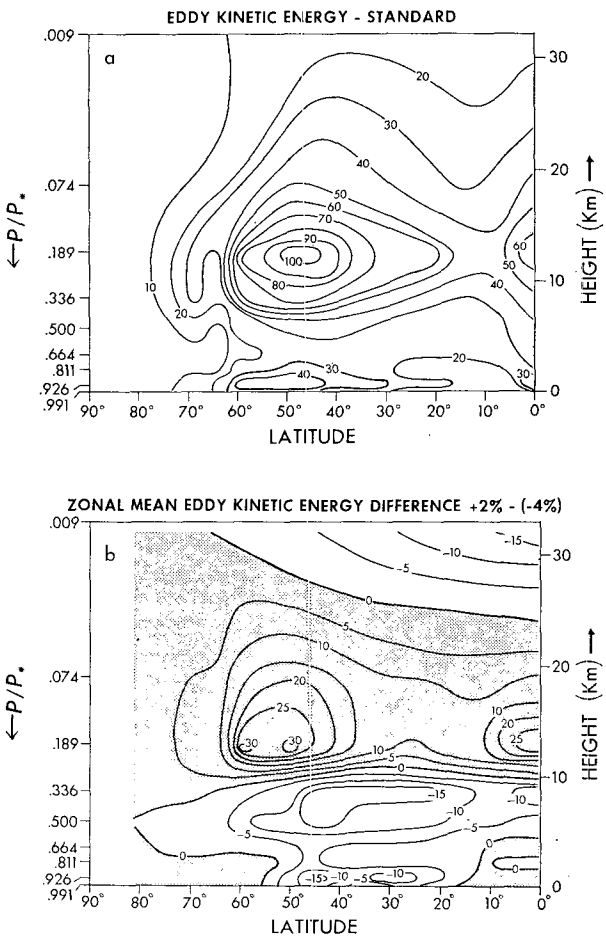

FIG. 12. Latitude-height distribution of zonal mean eddy kinetic energy for the 0% case (a) and for the difference between the +2% and −4% cases (b).

of the reasons why eddy kinetic energy increases above 300 mb in response to an increase in the solar constant. These responses of the model atmosphere to an increase in the solar constant are qualitatively similar to the responses resulting from an increase in the carbon dioxide concentration in air as described by MW75.

In subsection 4d, we pointed out that the poleward retreat of the region of snowfall due to the increase in the solar constant is much larger than the corresponding shift of the zone of maximum baroclinicity. This difference is found to be responsible for the remarkable reduction in the amount of snowfall resulting from the increase of the solar constant. Fig. 13 shows the latitudinal distribution of eddy kinetic energy at the 500 mb level for both the +2% and −4% cases. This result clearly indicates that a poleward shift of the latitude of maximum eddy kinetic energy does take place, but is very small, and, therefore, substantiates the statements made above.

f. Poleward transport of energy

The poleward transport of energy is one of the most important indicators of the atmospheric circulation. The latitudinal distribution of this quantity as well as its two components is shown in Fig. 14. In this figure $(C_pT+\phi)$ is dry static energy, (Lr) is latent energy, and $(C_pT+\phi+Lr)$ is moist static energy. Here, T, ϕ and r represent temperature, geopotential height and mixing ratio, respectively, and C_p and L denote the specific heat of air and latent heat of evaporation.

1) DRY STATIC ENERGY

According to Fig. 14a, the increased incoming solar radiation significantly decreases the poleward transport of dry static energy in middle latitudes. This result is consistent with the decrease of eddy kinetic energy in the lower troposphere where most of the heat transport by large-scale eddies takes place.

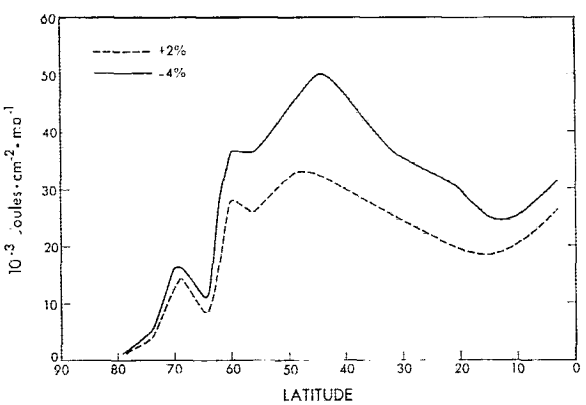

FIG. 13. Zonal mean eddy kinetic energy at the 500 mb level for the 2% and −4% cases.

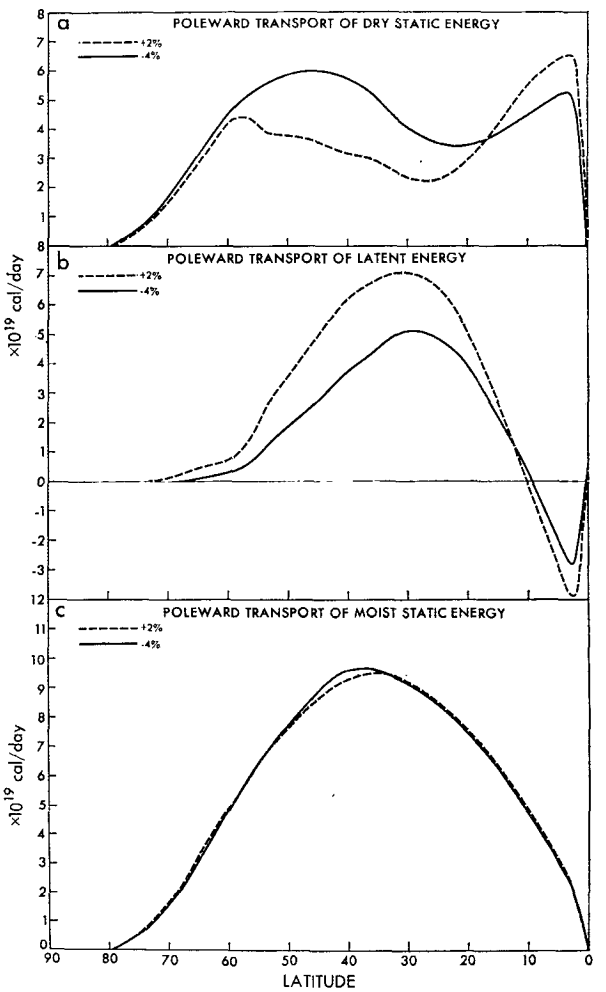

FIG. 14. (a) Poleward transport of dry static energy $(C_pT+\phi)$; (b) poleward transport of latent energy (Lr); and (c) poleward transport of moist static energy $(C_pT+\phi+Lr)$. Results are shown for both the 2% and −4% cases.

The reverse is true for low latitudes. The poleward transport of dry static energy increases significantly as a result of the increase of solar radiation. This increase is due to the reduction of the lapse rate in low latitudes, which is described in Section 4a. Such a reduction increases the difference in dry static energy between the upper and the lower troposphere and enhances the effectiveness of the Hadley cell in transporting dry static energy poleward.[3]

2) LATENT ENERGY

Fig. 14b shows a significant increase of poleward transport of latent energy in middle latitudes due to

[3] Upon further analysis, we found that this effect was more important in explaining the increase of poleward transport of dry static energy in low latitudes than the intensification of the Hadley cell as stated in MW75. It turns out that there is very little change in the strength of the Hadley cell in both MW75 and the current study.

the increase of solar radiation. This is opposite to the distribution of dry static energy shown in Fig. 14a and occurs despite the decrease of eddy kinetic energy previously mentioned. The above result is due to the general increase of atmospheric water vapor associated with an increase of temperature for the +2% case.

In the model tropics, the equatorward transport of latent heat for the +2% case is considerably larger than that for the −4% case. This difference is mainly due to the increase in the effectiveness of the Hadley cell in transporting moisture poleward resulting from the increase in the moisture content in air.

3) MOIST STATIC ENERGY

It is interesting to note in Fig. 14c that the poleward transports of moist static energy for both the +2% and −4% cases differ very little from each other. This is apparently due to the fact that the change in transport of dry static energy is almost completely compensated by a corresponding change in the transport of latent heat.

5. Summary and conclusions

In this study an attempt is made to analyze the effect of changing the solar constant from 1.92 to 2.04 ly min^{-1} in a highly simplified three-dimensional general circulation model. The main results of this study may be summarized as follows:

1) In general, the temperature of the model troposphere increases with increasing solar constant. This increase is most pronounced in the lower troposphere of higher latitudes due to the effects of snow-cover feedback and the suppression of vertical mixing by a stable stratification. It was found that the dependence of the surface temperature on the solar constant decreases with increasing solar constant. This is because the effects of the snow-cover feedback mechanism decrease as the snow-cover area shrinks. It is encouraging that the results described above qualitatively agree with those obtained earlier by Budyko (1969) and Sellers (1969). However, there are significant quantitative differences among these results. In view of the many drastic assumptions which are made in the present study, it is not justified to conclude that the quantitative aspect of the present results are superior to the earlier ones simply because the model involves a lesser degree of parameterization.

2) It is found that the intensity of the hydrologic cycle of the model is extremely sensitive to the change in the solar constant. According to our analysis, the percentage increase of the mean rate of evaporation is about 4.5 times as much as that of the solar constant. The following factors are identified to be responsible for increasing the rate of evaporation and thus enhancing the intensity of the hydrologic cycle:

(i) The net upward terrestrial radiation at the surface of the model earth decreases with increasing solar constant. Together with the increase of the net downward solar radiation at the surface, this decrease makes more energy available for evaporation. The decrease in net upward terrestrial radiation mentioned above occurs because the downward terrestrial radiation increases. This is due to the increase in the moisture content in air and to the reduction of the lapse rate in low latitudes where moist convection mainly controls the static stability of the model atmosphere.

(ii) The derivative of saturation vapor pressure with respect to temperature increases markedly with increasing temperature. Therefore, the vertical gradient of saturation vapor pressure increases more than the vertical temperature gradient responding to the increase in surface temperature. This implies that the Bowen ratio decreases with increasing surface temperature. Accordingly, larger proportions of radiative energy available at the surface are used for evaporation rather than consumed by the sensible heat flux.

3) The latitudes of maximum snowfall and maximum snow accumulation retreat poleward in response to the increase in the solar constant. Furthermore, the total amounts of snowfall and snow accumulation decrease markedly with increasing insolation. This decrease partly results from the poleward shift of the zone of subfreezing surface temperature away from the belt of maximum baroclinic instability where intense vertical motion prevails. One can speculate that the development of a thick ice cap during past ice ages results from the reverse process, i.e., overlapping of the zone of subfreezing surface temperature with the baroclinic zone.

4) In the lower troposphere, the magnitude of the eddy kinetic energy decreases with increasing solar constant. This layer of decrease approximately corresponds with the layer of a reduced meridional temperature gradient and increased static stability. Conversely, there is an increase of eddy kinetic energy in the upper troposphere and the lower stratosphere where the static stability decreases significantly with increasing solar constant.

As we pointed out in the previous carbon dioxide study, one should remember that the current investigation is, again, carried out using a zonal mean fixed cloud distribution. In view of the fact that the distribution of relative humidity, which can influence cloud distribution, changed significantly in response to the change in the solar constant, it is possible that the present results may be altered considerably if the assumption of fixed cloudiness is replaced by a cloud prediction scheme. It should also be recalled that the present model contains such features as a swamp ocean, idealized topography, and annual mean insolation, any one of which is capable of changing the sensitivity of the model climate. Because of these limitations, this study should not be re-

garded as a quantitative investigation of climate sensitivity to changes of solar radiation but rather as a means of identifying some of the important processes which control this response.

Acknowledgments. The authors are indebted to Dr. J. Smagorinsky who has given them many valuable suggestions and wholehearted support during the course of the entire sensitivity study. Thanks are due to I. Held and M. Suarez and Dr. S. Fels who gave constructive comments on the original manuscript. We are also grateful to M. Stern for her help in the analysis of the results. Finally, we would like to express our appreciation to E. Thompson, P. Tunison and J. Conner for their assistance in preparing the manuscript.

APPENDIX A

White Earth Solution

At the end of Section 3, it was stated that if the present general circulation model is perturbed too greatly by either external forcing or extreme initial conditions, the resulting quasi-equilibrium state could be radically different from the ones obtained in this investigation as well as in the previous carbon dioxide study. In order to get an idea of the nature of this different state, a test case (referred to here as the White Earth case) was integrated for a period of 310 model days starting from a resting, isothermal atmosphere of 220 K. To be consistent with this starting temperature, we assumed that the ocean was occupied by solid ice and that the continent was covered by a uniform snow depth of 1 cm water equivalent. All other features of the model were unchanged and the value of the solar constant was taken to be the standard value, namely 2 ly min^{-1}. The low value of temperature implies that the initial surface albedo will be set to 70% everywhere in the computational region. It is, therefore, of interest to see whether the mean temperature field increases or decreases with time from its initial value.

According to the above integration, the mean temperature decreased to about 193 K. This result suggests that once an ice- or snow-covered earth condition is imposed upon the model climate, it never recovers from this state. Also, analysis of the hydrologic cycle indicates that snowfall slightly exceeds sublimation at every latitude circle due to a general reduction of the moisture-holding capacity of the model atmosphere with time. In order to economize on computer time, we did not attempt to reach a quasi-steady-state equilibrium for this case but rather terminated the run when the mean temperature began to level off. Fig. A1 shows the distribution of zonal mean temperature which represents a time average over the last 60 days of this run. It is interesting to compare this temperature distribution with that for the 0% case given in Fig. 3a. In general for the White Earth case, the temperature throughout the entire model troposphere is much colder than that for the 0% case. On the other hand, in the stratosphere there is relatively little difference between the two results. Accordingly, the height of the tropopause for the White Earth case is located at about the 500 mb level and is much lower than the corresponding tropopause height for the standard case. The region of maximum meridional temperature gradient appears to be confined within the lower tropospheric layer below the 664 mb level. This is also true for the region of maximum activity of baroclinic disturbances.

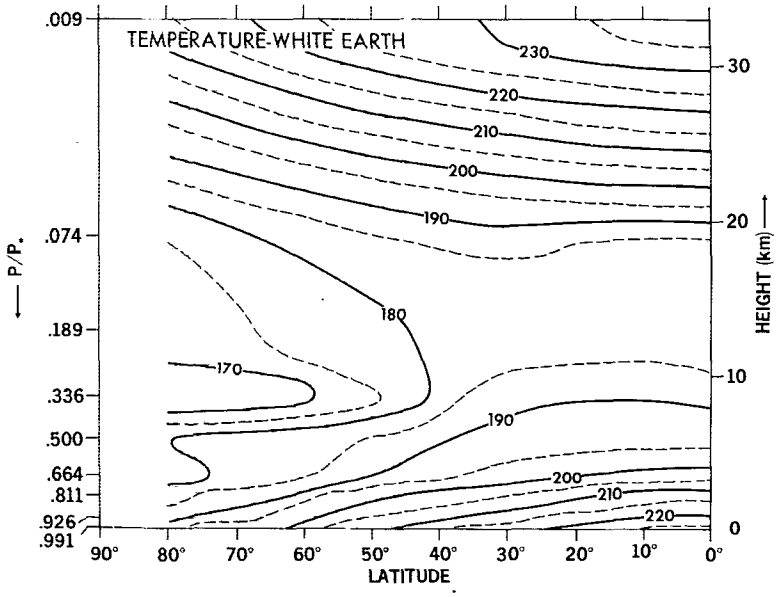

FIG. A1. Latitude-height distribution of zonal mean temperature for the White Earth case. Units are K.

APPENDIX B

Solar Constant and Terrestrial Surface Radiation

In Section 4c, it is shown that the net upward terrestrial radiation decreases with increasing solar radiation. It is stated that this reduction results from the increase of downward radiation due to an increase of atmospheric moisture content in air, and a decrease of static stability in middle and low latitudes where moist convection predominates. These explanations emerged not only from the analysis described in the main text of the paper but also from the study of radiative, convective equilibrium which is described below.

The radiative, convective model of the atmosphere used in this Appendix is very similar to the one-dimensional models developed by Manabe and Strickler (1964), and Manabe and Wetherald (1967) with the exception of the scheme for computing radiative transfer. The radiative scheme used here was originally proposed by Rodgers and Walshaw (1966) and was modified by Stone and Manabe (1968).

Four series of computations of radiative, convective equilibrium were carried out for four different values of the solar constant. Each series is identified by abbreviated symbols as listed below. The method of specifying the humidity distribution and the critical lapse rate for convection, which are adopted for each series, are contained in the parentheses:

(1) R-6.5 (Fixed absolute humidity; critical lapse rate, 6.5°C km^{-1}).
(2) H-6.5 (Fixed relative humidity; critical lapse rate, 6.5°C km^{-1}).
(3) R-MA (Fixed absolute humidity; critical lapse rate, moist-adiabatic).
(4) H-MA (Fixed relative humidity; critical lapse rate, moist-adiabatic).

Vertical distributions of absolute and relative humidity which are used for these computations are given by Manabe and Wetherald (1967). In each series net upward terrestrial radiation at the earth's surface is computed for four different values of the solar constant and is plotted in Fig. B1.

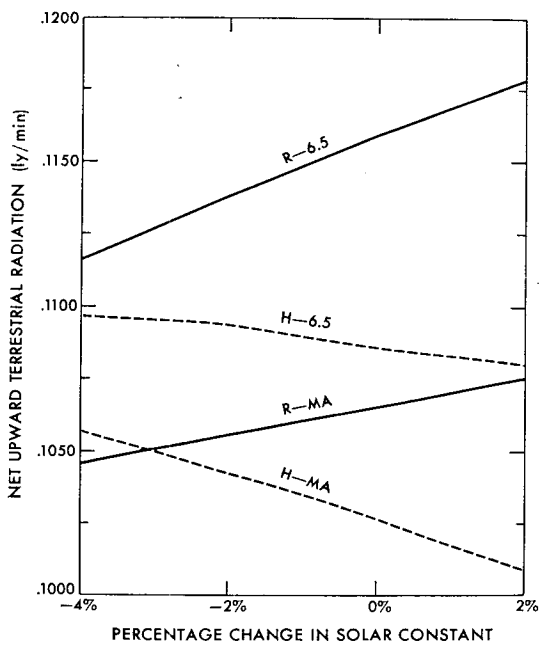

FIG. B1. Results from the computation of radiative, convective equilibrium. Ordinate: net upward terrestrial radiation at the earth's surface of the model in units of ly min^{-1}; abscissa: percentage deviation of the solar constant from the standard value. R-6.5, H-6.5, R-MA and H-MA denote the different series of experiments. See text for further description of these series.

It has been pointed out that the atmosphere tends to maintain a certain climatological distribution of relative humidity despite the substantial change in temperature with time (Möller, 1963). Therefore, by comparing the results from the H-6.5 series (with fixed relative humidity) with those from the R-6.5 series (with fixed absolute humidity), one can get some idea of how the change in moisture content in air affects the dependence of surface radiative flux on the magnitude of the solar constant. In Section 4a, it is pointed out that the lapse rate in lower latitudes of our general circulation model is close to the moist adiabatic value because of the predominance of moist convection. This implies that the lapse rate in the model troposphere decreases with increasing air temperature. Therefore, by comparing the results from the H-MA series (with moist adiabatic lapse rate) with those from the H-6.5 series (with constant lapse rate), one can determine how the dependence of lapse rate upon temperature affects the relationship between the solar constant and surface flux of radiation. According to Fig. B1, the net upward terrestrial radiation at the earth's surface of the model 1) increases significantly for the R-6.5 series, 2) decreases slightly for the H-6.5 series, and 3) decreases significantly for the H-MA series responding to the increase in the solar constant. These results appear to be consistent with the explanations for the reduction of upward surface radiation, which are stated at the beginning of this appendix.

REFERENCES

Budyko, M. I., 1956: Teplovoi Balans Zemnoi Poverkhnosti [English translation: N. A. Stepanova, 1958: *The Heat Balance of the Earth's Surface*, Washington, D.C., Office of Technical Services, U. S. Department of Commerce, 259 pp], Leningrad, Gidrometeor., 255 pp.

——, 1969: The effect of solar radiation variations on the climate of the Earth. *Tellus*, **21**, 611–619.

Held, I. M., and M. J. Suarez, 1974: Simple albedo feedback models of the icecaps. *Tellus*, **26**, 613–629.

Holloway, J. L., Jr., M. J. Spelman and S. Manabe, 1973: Latitude-longitude grid suitable for numerical time integration of a global atmospheric model. *Mon. Wea. Rev.*, **101**, 69–78.

Manabe, S., 1969: Climate and the ocean circulation: I. The atmospheric circulation and the hydrology of the earth's surface. *Mon. Wea. Rev.*, **97**, 739–774.

——, and K. Bryan, 1969: Climate calculations with a combined ocean-atmosphere model. *J. Atmos. Sci.*, **26**, 786–789.

——, and R. F. Strickler, 1964: Thermal equilibrium of the atmosphere with a convective adjustment. *J. Atmos. Sci.*, **21**, 361–385.

——, and R. T. Wetherald, 1967: Thermal equilibrium of the atmosphere with a given distribution of relative humidity. *J. Atmos. Sci.*, **24**, 241–259.

——, and ——, 1975: The effects of doubling the CO_2 concentration on the climate of a general circulation model. *J. Atmos. Sci.*, **32**, 3–15.

Möller, F., 1963: On the influence of changes in the CO_2 concentration in air on the radiation balance of the earth's surface and on the climate. *J. Geophys. Res.* **68**, 3877 3886.

Oort, A. H., and E. M. Rasmusson, 1971: Atmospheric circulation statistics. NOAA Prof. Paper **5**, U. S. Government Printing Office, Washington, D. C., 233 pp.

Rodgers, C. D., and D. C. Walshaw, 1966: The computation of infra-red cooling rate in planetary atmospheres. *Quart. J. Roy. Meteor. Soc.*, **92**, 67–92.

Sellers, W. D., 1969: A global climate model based on the energy balance of the earth-atmosphere system. *J. Appl. Meteor.*, **8**, 392–400.

Simpson, G. C., 1934: World climate during the quaternary period. *Quart. J. Roy. Meteor. Soc.*, **60**, 425–478.

Smagorinsky, J., 1960: On the dynamical prediction of large-scale condensation by numerical methods. *Physics of Precipitation*, Geophys. Monogr. No. 5, Amer. Geophys. Union, 71–78.

——, 1963: General circulation experiments with the primitive equations: I. The basic experiment. *Mon. Wea. Rev.*, **91**, 99–164.

Stone, H. M., and S. Manabe, 1968: Comparison among various numerical models designed for computing infrared cooling. *Mon. Wea. Rev.*, **96**, 735–741.